

Electronic Supplementary Information

Aryl-substituted-indanone end-capped nonfullerene acceptors for organic solar cells with a low nonradiative loss†

Meiling Xie,^{‡ab} Yanan Shi,^{‡ab} Hao Zhang,^{ab} Junxiu Pan,^{ac} Jianqi Zhang,^a Zhixiang

Wei,^{ab} and Kun Lu^{*ab}

^a *Chinese Academy of Sciences (CAS) Key Laboratory of Nanosystem and Hierarchical Fabrication, CAS Center for Excellence in Nanoscience, National Center for Nanoscience and Technology, Beijing 100190, China. E-mail: lvk@nanoctr.cn*

^b *University of Chinese Academy of Sciences, 100049 Beijing, China*

^c *Tianjin Key Laboratory of Molecular Optoelectronic Sciences, Department of Chemistry, School of Science, Tianjin University, Tianjin 300072, China*

Compound 3-2 (IC-N): was synthesized by similar procedure as compound 3-1 between compound 1 and compound 2-2. The final product were obtained as red solid.

^1H NMR (400 MHz, CDCl_3) δ 8.76 (d, $J = 8.3$ Hz, 1H), 8.12 (s, 1H), 8.05 (dd, $J = 8.2, 1.6$ Hz, 1H), 7.97 (d, $J = 7.4$ Hz, 2H), 7.75 (d, $J = 8.2$ Hz, 1H), 7.57 (d, $J = 8.2$ Hz, 2H), 7.51 (d, $J = 7.1$ Hz, 2H), 3.81 (s, 2H).

Compound 3-3 (IC-B): was synthesized by similar procedure as compound 3-1 between compound 1 and compound 2-3. The final product were obtained as brown solid. ^1H NMR (400 MHz, CDCl_3) δ 8.70 (d, $J = 8.4$ Hz, 1H), 8.18 (d, $J = 1.5$ Hz, 1H), 8.12 (dd, $J = 8.4, 1.8$ Hz, 1H), 7.73 – 7.66 (m, 2H), 7.57 – 7.49 (m, 3H), 3.76 (d, $J = 8.2$ Hz, 2H).

Compound 5-1 (BTP-C9-ICT): Compound 4 (100mg; 0.088mmol) and compound 3-1 (146mg, 0.53mmol) were dissolved into dry chloroform (30mL) in a three-neck flask. The solution was flushed with nitrogen for 20 min. After 0.4mL pyridine were added, the resulting solution was refluxed and stirred for 12 h under nitrogen. After cooling to room temperature, the reaction mixture was poured into water and extracted several times with chloroform. Then the solvent was removed under reduced pressure, and the crude product was purified by column chromatography on silica gel to yield BTP-C9-ICT as black solid. ^1H NMR (400 MHz, CDCl_3) δ 9.14 (s, 2H), 8.69 (d, $J = 8.0$ Hz, 2H), 8.12 (s, 2H), 7.96 (d, $J = 8.1$ Hz, 2H), 7.58 (d, $J = 2.6$ Hz, 2H), 7.48 (d, $J = 4.7$ Hz, 2H), 7.19 (s, 2H), 4.80 (s, 4H), 3.22 (s, 4H), 2.18 (s, 2H), 1.88 (s, 4H), 1.54 (d, $J = 19.1$ Hz, 6H), 1.33 (d, $J = 36.8$ Hz, 22H), 0.99 (ddd, $J = 51.2, 32.3, 9.1$ Hz, 34H), 0.76 – 0.59 (m, 12H). MALDI-TOF MS (m/z):1599.945.

Compound 5-2 (BTP-C9-ICN): was synthesized by similar procedure as compound 5-1 between compound 4 and compound 3-2. The final product were obtained as black solid. ^1H NMR (400 MHz, CDCl_3) δ 9.23 (s, 2H), 8.84 (d, $J = 8.2$ Hz, 2H), 8.09 (d, $J = 1.3$ Hz, 2H), 7.93 (ddd, $J = 24.2, 19.4, 8.3$ Hz, 8H), 7.65 – 7.54 (m, 4H), 7.54 – 7.45 (m, 4H), 4.80 – 4.65 (m, 4H), 3.27 (t, $J = 7.6$ Hz, 4H), 2.18 – 2.06 (m, 2H), 1.98 – 1.84 (m, 4H), 1.54 (d, $J = 10.0$ Hz, 6H), 1.32 (dd, $J = 25.3, 19.8$ Hz, 20H), 1.21 – 0.70 (m, 36H), 0.61 (ddd, $J = 19.2, 13.9, 7.2$ Hz, 12H). MALDI-TOF MS (m/z):1688.069.

Compound 5-3 (BTP-C9-ICB): was synthesized by similar procedure as compound 5-1 between compound 4 and compound 3-3. The final product were obtained as black

solid. ^1H NMR (400 MHz, CDCl_3) δ 9.19 (s, 2H), 8.78 (d, $J = 8.3$ Hz, 2H), 8.16 (t, $J = 6.7$ Hz, 2H), 8.01 (dd, $J = 8.3, 1.7$ Hz, 2H), 7.72 (t, $J = 7.9$ Hz, 4H), 7.57 – 7.49 (m, 6H), 4.77 (d, $J = 7.5$ Hz, 4H), 3.32 – 3.20 (m, 4H), 2.15 (s, 2H), 1.91 (dd, $J = 14.9, 7.7$ Hz, 4H), 1.71 (s, 8H), 1.59 – 1.49 (m, 4H), 1.39 – 1.22 (m, 26H), 0.94 (ddd, $J = 37.0, 13.2, 6.7$ Hz, 24H), 0.67 (ddd, $J = 15.6, 13.6, 7.3$ Hz, 12H). MALDI-TOF MS (m/z):1587.983.

2. Methods and measurements

Optical and electrical Properties. ^1H NMR was obtained on a Bruker Avance III 400 NMR Spectrometer (operating at 400 MHz, using CDCl_3 as solvent using tetramethylsilane as internal standard). The UV-vis absorption were measured by Shimadzu UV-3600 spectrophotometer. The electrochemical cyclic voltammetry (CV) was conducted an electrochemical workstation (VMP3 Biologic, France) with a Pt disk coated with blend film, a Pt plate, and an Ag^+/Ag electrode acting as the working, counter, and reference electrodes, respectively, in a 0.1 mol/L tetrabutylammonium phosphorus hexafluoride (Bu_4NPF_6) acetonitrile solution. The experiments were calibrated with the standard ferrocene/ferrocenium (Fe) redox system and assumption that the energy level of Fe is 4.8 eV below vacuum.

Device fabrication. For PM6:BTP-C9-ICB, PM6:BTP-C9-ICN, and PM6:BTP-C9-ICT-based binary OSCs, conventional devices were fabricated by using an structure of ITO/PEDOT:PSS/active layer/PFNBr/Al, where PEDOT:PSS and PFNBr were used as hole-transport and electron-transport interlayer respectively. The ITO glass substrates were cleaned sequentially under sonication with detergent, deionized water, ethanol and isopropyl alcohol. After oxygen plasma cleaning for 15 minutes, the PEDOT:PSS layer was deposited by spin-coating under 3500 rpm for 30 s on top of the ITO substrate with thermal annealed for 15 minutes at 150 °C. The blended solution was prepared by mixing PM6 and acceptors in a 1:1.2 weight ratio into chloroform (CF) at a total concentration of 14 mg/ml and with the addition of a small amount of chloronaphthalene (0.5 %, v/v). The blend solution was spincoated at 2500 rpm for 30 s to form a thin film on the substrate. Then the ETLs dissolved in

methanol at a concentration of 0.5 mg/ml was spun onto the blend layer at 3000 rpm for 30 s. Finally, 80 nm-thick Al were deposited onto the ETLs layer under vacuum at a pressure of 3×10^{-6} . For PM6:Y6, PM6:Y6:BTP-C9-ICT-based binary and ternary OSCs, devices were fabricated under similar conditions as PM6:BTP-C9-ICX-based devices apart from the spincoating rate of blend films (3000 rpm). Except for the fabrication of PEDOT:PSS layer, the other processes were all carried out in a nitrogenfilled glovebox. Device area of each cell was approximately 4mm². The *J-V* measurements were conducted in glove box using the solar simulator (SS-F5-3A, Enlitech) under AM 1.5 G (100 mWcm⁻²). The light intensity was calibrated with the standard silicon solar cell (SRC-2020). The EQE measurements were performed with the integrated system (QE-R, QER3011, Enlitech).

FTPS-EQE and EL measurements. Fourier-transform photocurrent spectroscopy external quantum efficiency (FTPS-EQE) measurements were carried out by an integrated system (PECT600, Enlitech). Electroluminescence (EL) measurements were obtained by applying an external voltage/current source through the device REPS, Enlitech.

Mobility measurements. Hole and electron mobilities were measured by the space-charge limited current (SCLC) method with hole-only devices and electron-only devices. The hole-only devices adopted ITO/PEDOT:PSS/active layer/MoOx/Ag structure, while electron-only devices adopting ITO/ZnO/active layer/PFNBr/Al structure. The active layers for these two devices were spincoated under the same condition as that of solar cells. *J-V* curves in the range of 0 to 5 V were gained by Keithley 2400 source-measure unit in the dark condition. The mobilities were obtained by fitting *J-V* curves with the equation:

$$J = \frac{9\varepsilon_r\varepsilon_0\mu_0V^2}{8L^3} \exp\left(\beta\sqrt{\frac{V}{L}}\right)$$

where *J* is the current density, *L* is the thickness of the active layer, μ is the mobility,

ϵ_0 is the vacuum dielectric constant, ϵ_r is the relative dielectric constant of the transport medium, $V (= V_{app} - V_{bi})$ is the internal voltage, where V_{app} is the applied voltage and V_{bi} is the built-in voltage.

Morphology crystallization characterization. Atomic force microscopy (AFM) images of the blend films were obtained from the devices directly on a VEECO Dimension 3100 atomic force microscope working under ScanAsys mode. Grazing incidence wide-angle X-ray scattering (GIWAXS) experiments were conducted at XEUS SAXS/WAXS equipment.

Contact angle measurements. Contact angles were measured with a contact angle meter (GBX DIGIDROP). Droplets of water, diiodomethane (DIM) were dripped onto the pure films of acceptors. Then the surface free energy was calculated by Owens-Wendt method.¹ The surface energy could be divided into dispersive and polar components.

$$\gamma = \gamma^d + \gamma^p$$

The values of γ^d and γ^p can be solved though combining two equations obtained by contact angle measurements of two different solvents.

$$(1 + \cos\theta)\gamma_L = 2\sqrt{\gamma_s^d \gamma_L^d} + 2\sqrt{\gamma_s^p \gamma_L^p}$$

where θ is the contact angle of a specific solvent, γ_L is the surface energy of the solvent, γ_s^d and γ_s^p present the dispersive and polar surface energy of the solid film, respectively; γ_L^d and γ_L^p represent the dispersive and polar surface energy of the solvent, respectively.

The Flory–Huggins interaction parameter $\chi_{donor-acceptor}$ is derived using the empirical equation:²

$$\chi_{donor-acceptor} = K \left(\gamma_{donor}^{1/2} - \gamma_{acceptor}^{1/2} \right)^2$$

where K is a positive constant; γ_{donor} and $\gamma_{acceptor}$ represent the surface energies of the pure films.

Energy loss analysis.

a) Based on Shockley-Queisser limit theory, the E_{loss} in OSCs originates from three parts as shown in Equation 1: ³

$$\begin{aligned}
 E_{loss} &= E_g - qV_{oc} \\
 &= (E_g - qV_{oc}^{SQ}) + (qV_{oc}^{SQ} - qV_{oc}^{rad}) + (qV_{oc}^{rad} - qV_{oc}) \\
 &= (E_g - qV_{oc}^{SQ}) + q\Delta V_{oc}^{rad, belowgap} + q\Delta V_{oc}^{non-rad} \\
 &= \Delta E_1 + \Delta E_2 + \Delta E_3 \quad (1)
 \end{aligned}$$

where q is the elementary charge; V_{oc}^{SQ} is the maximum voltage by the S-Q limit; V_{oc}^{rad} is the open-circuit voltage when there is only radiative recombination in the device; $\Delta V_{oc}^{rad, belowgap}$ is the voltage loss of radiative recombination below the bandgap; $\Delta V_{oc}^{non-rad}$ is the voltage loss due to non-radiative recombination. The photovoltaic bandgap energy (E_g^{PV}) obtained from the derivative of the EQE spectrum was used to determined bandgap.⁴

b) The detailed calculating methods of energy loss are as follows.^{5, 6} The V_{oc} for any type of solar cells is determined by this formula:

$$V_{oc} = \frac{kT}{q} \ln \left(\frac{J_{sc}}{J_0} + 1 \right) \quad (2)$$

where k is the Boltzmann constant, T is the Ketemperature, and q is the elementary charge.

The expression of short circuit current (J_{sc}) and dark current (J_0) are given by:⁷

$$J_{sc} = q \cdot \int_0^{\infty} EQE_{PV}(E) \phi_{AM1.5G}(E) dE \quad (3)$$

$$J_0 = \frac{q}{EQE_{EL}} \cdot \int_{E_g}^{\infty} EQE_{PV}(E) \phi_{BB}(E) dE \quad (4)$$

where EQE_{EL} is the radiative quantum efficiency of the solar cell with injected currents in dark condition.

When there is only radiative recombination in the device, $EQE_{EL} = 1$. Based on S-Q theory, the general quantum efficiency can be defined as:

$$EQE_{PV}^{SQ}(E) = 1, \quad E \geq E_g \quad ; \quad EQE_{PV}^{SQ}(E) = 0, \quad E < E_g \quad (5)$$

Accordingly, the V_{oc}^{SQ} can be calculated by the equation:

$$V_{oc}^{SQ} = \frac{kT}{q} \ln \left(\frac{J_{sc}}{J_0^{SQ}} + 1 \right) = \frac{kT}{q} \ln \left(\frac{q \cdot \int_0^{\infty} EQE_{PV}(E) \phi_{AM1.5G}(E) dE}{q \cdot \int_{E_g}^{\infty} \phi_{BB}(E) dE} + 1 \right) \quad (6)$$

Likewise, the V_{oc}^{rad} can be calculated as follow:

$$V_{oc}^{rad} = \frac{kT}{q} \ln \left(\frac{J_{sc}}{J_0^{rad}} + 1 \right) = \frac{kT}{q} \ln \left(\frac{q \cdot \int_0^{\infty} EQE_{PV}(E) \phi_{AM1.5G}(E) dE}{q \cdot \int_0^{\infty} EQE_{PV}(E) \phi_{BB}(E) dE} + 1 \right) \quad (7)$$

where $\phi_{BB}(E)$ is the black body spectrum, given by:

$$\phi_{BB}(E) = \frac{2\pi E^2}{h^3 c^2} \frac{1}{\left[\exp\left(\frac{E}{kT}\right) - 1 \right]} \approx \frac{2\pi E^2}{h^3 c^2} \exp\left(\frac{-E}{kT}\right) \quad (8)$$

where h is Planck's constant, and c is the speed of light in vacuum.

c) In summary, we can obtain these three terms of energy losses from experiments and calculations:

$$\Delta E_1 = E_g - qV_{oc}^{SQ}$$

$$\Delta E_2 = qV_{oc}^{SQ} - qV_{oc}^{rad}$$

And the nonradiative energy loss (ΔE_3) can be calculated by EQE_{EL} measurements:

$$\Delta E_3 = -kT \ln(EQE_{EL})$$

Photoluminescence measurements

The photoluminescence quantum yield (PLQY) values were recorded on the Steady/Transient State Fluorescence Spectrometer (FLS 1000, Edinburgh Instruments, UK).

The relationship between PLQY and electroluminescence external quantum efficiency (EQE_{EL}) was determined by the following equation:⁸

$$EQE = f_{e-h} \times \beta \times \eta_{PLQY} \times f_{outcoupling}$$

where f_{e-h} is the probability of balanced charge injection (when the numbers of electrons and holes injected are equal, this factor is equal to 1), β is the probability

of forming a correlated electron-hole pair or exciton from each pair of injected carriers, η_{PLQY} is the photoluminescence quantum yield (PLQY), and $f_{\text{outcoupling}}$ is the optical outcoupling coefficient.

3. Figures and tables

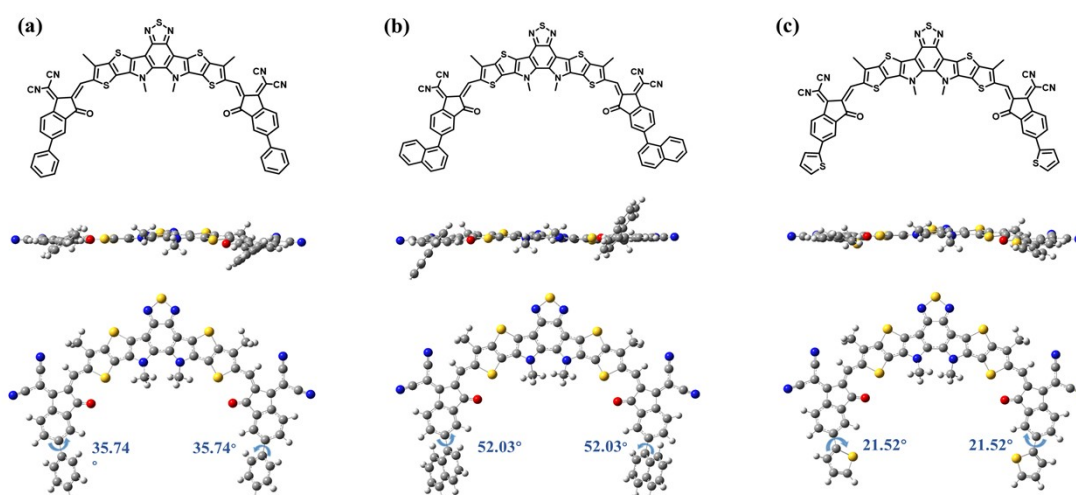


Fig. S1 Simulated molecular geometries by DFT calculations for simplified molecules of a) BTP-C9-ICB, b) BTP-C9-ICN, and c) BTP-C9-ICT.

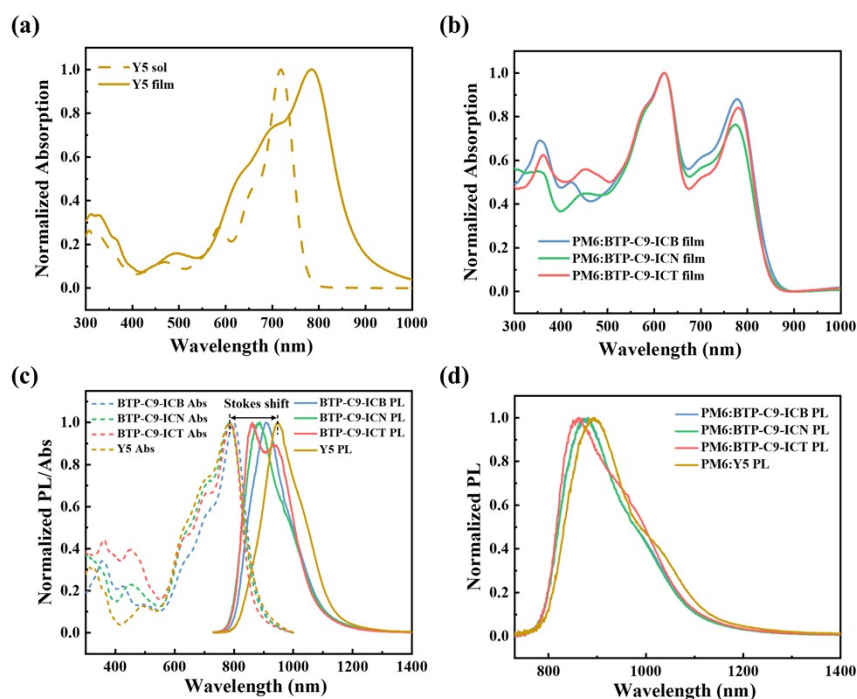


Fig. S2 Normalized absorption spectra of a) Y5 in solutin and film state, b) blend film based on three acceptors; normalized PL spectra of c) pure film and d) blend film excited at 710 nm.

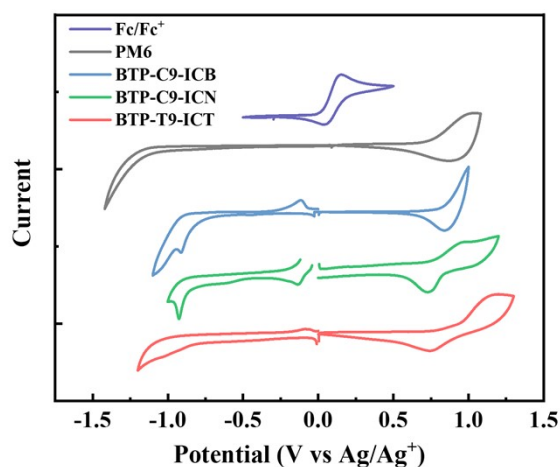


Fig. S3 Electrochemical cyclic voltammetry (CV) curves of these molecules measured in 0.1 mol L⁻¹ Bu₄NPF₆ acetonitrile solutions.

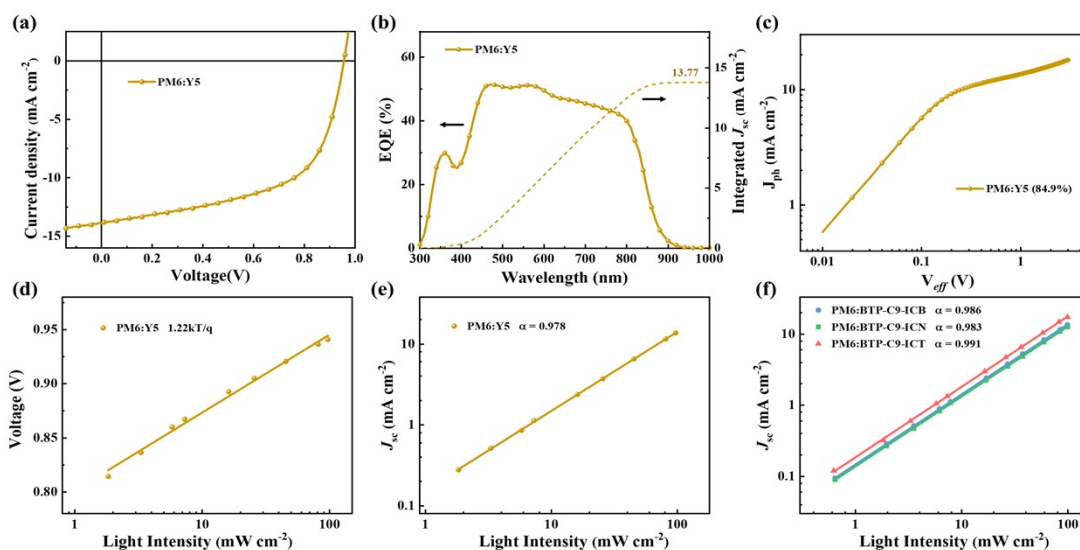


Fig. S4 a) J-V curves and b) EQE spectra (solid line) and integrated J_{sc} values (dashed line) of the optimal devices; c) photocurrent density (J_{ph}) as a function of effective voltage (V_{eff}); d) dependence of V_{oc} on the light intensity for optimized PM6:Y5-based device; e-f) dependence of J_{sc} on the light intensity for optimized PM6:Y5 and PM6:BTP-C9-ICX-based devices.

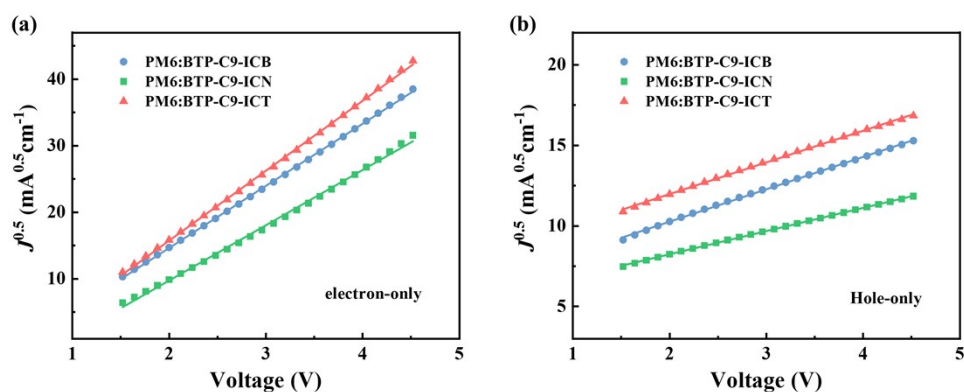


Fig.S5 $J^{0.5}$ -V curves of (a) electron-only and (b) hole-only devices.

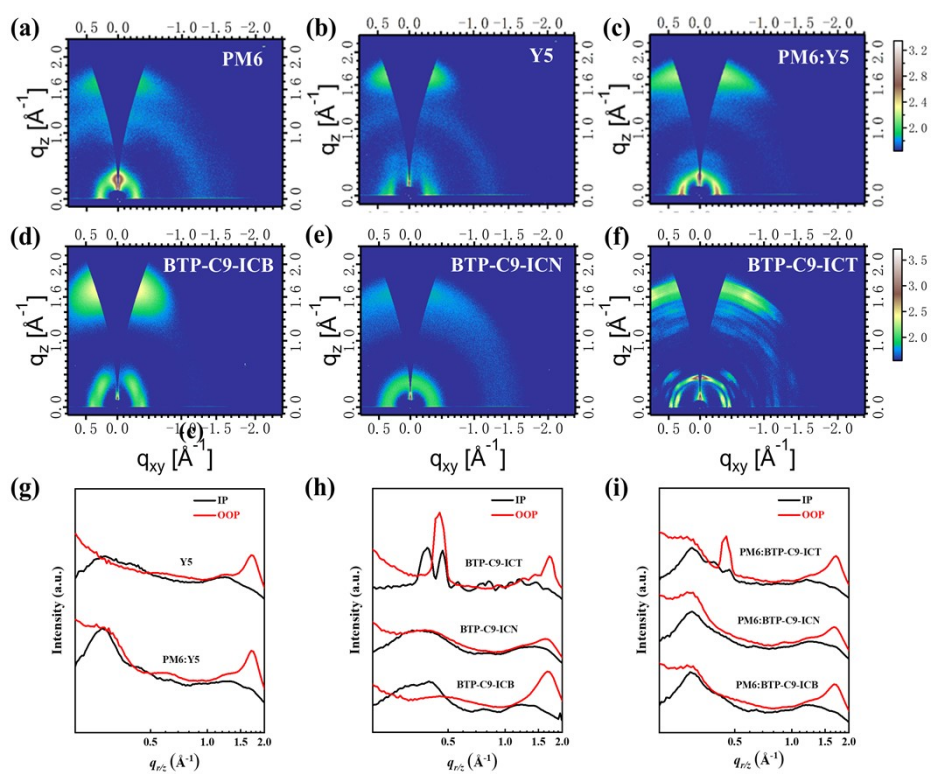


Fig. S6 Two-dimensional GIWAXS patterns of a) PM6, b) Y5, c) PM6:Y5 blend film, d) BTP-C9-ICB, e) BTP-C9-ICN, f) BTP-C9-ICT pure film; g-i) profiles of scattering intensity of the GIWAXS pattern.

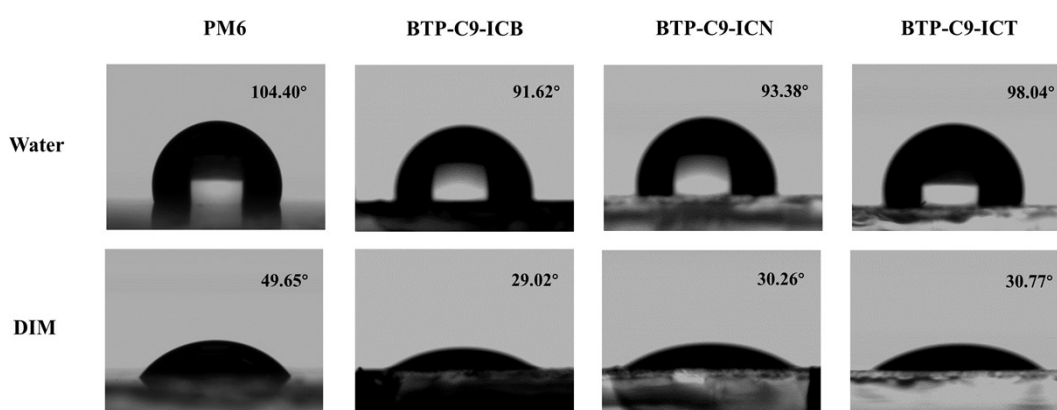


Fig. S7 Contact angle images of water and diiodomethane (DIM) droplets on the pure films of PM6 and our three acceptors.

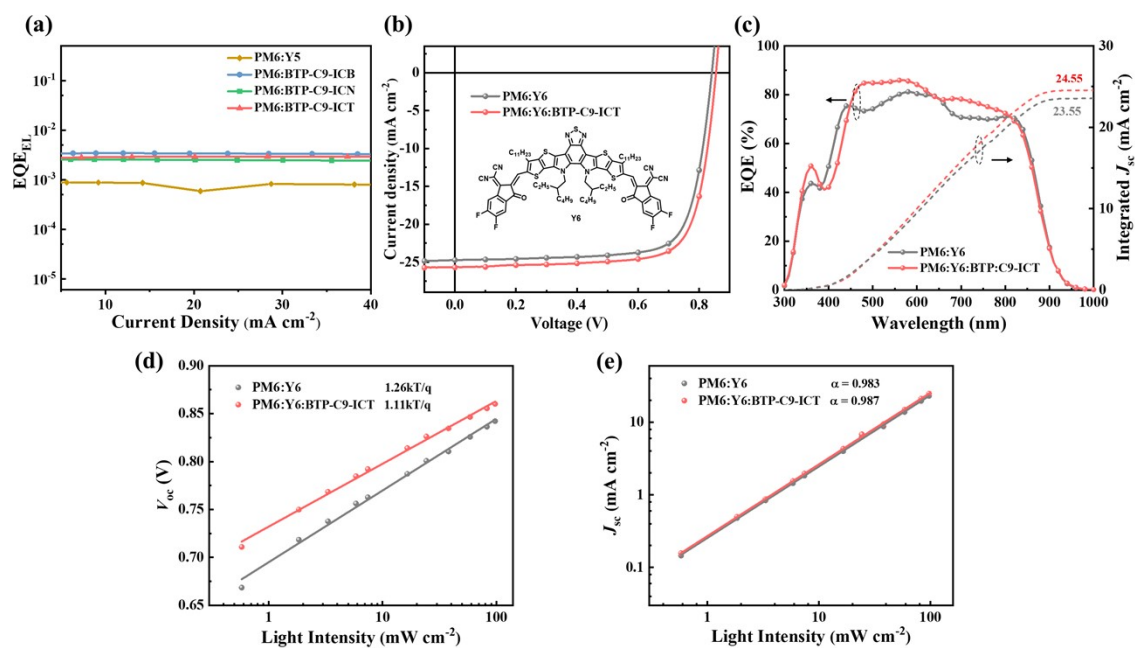
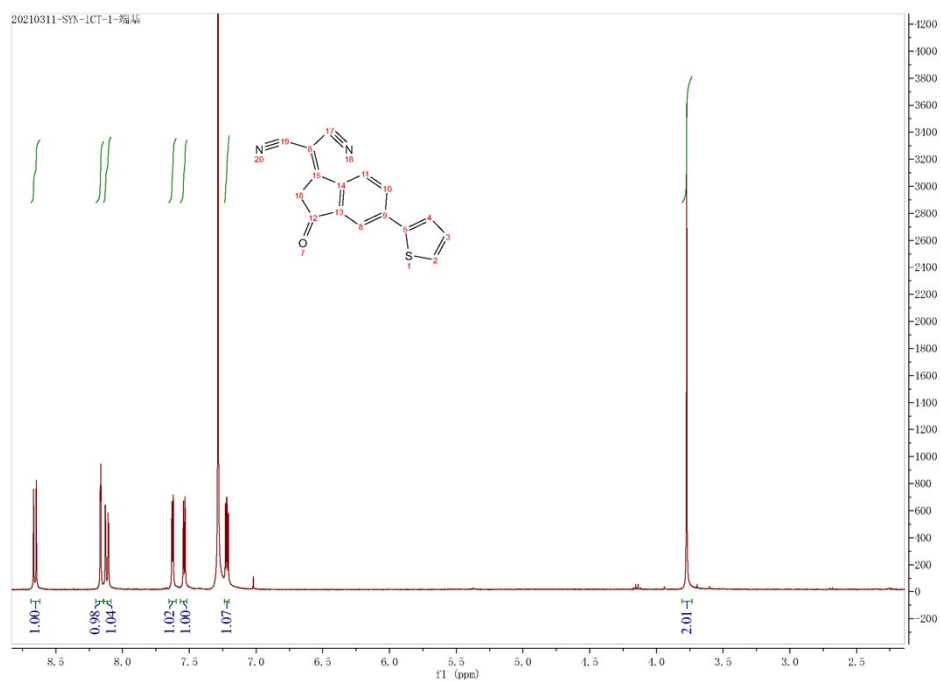
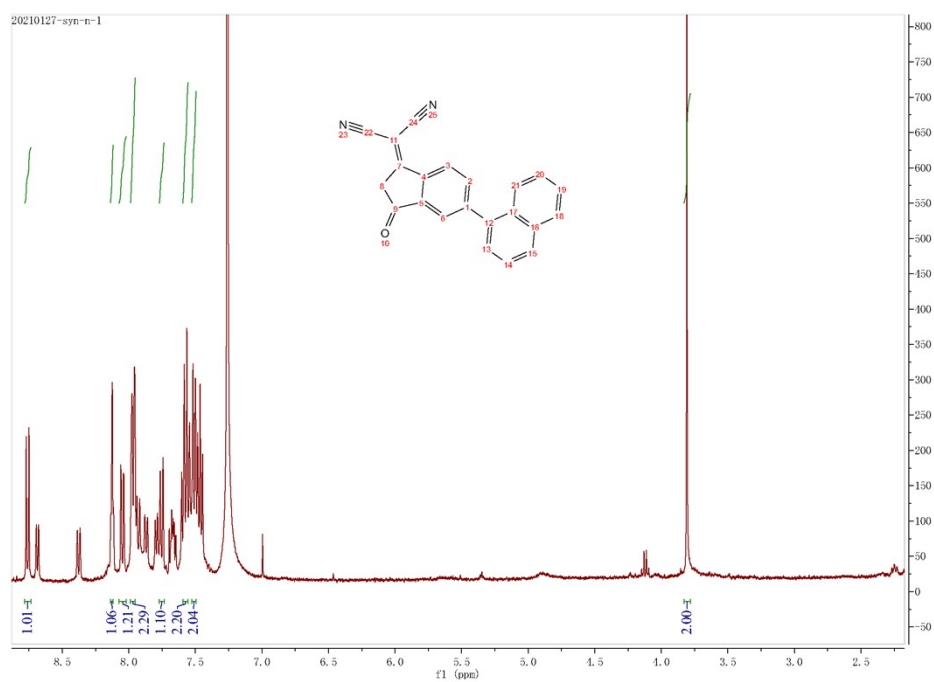


Fig. S8 (a) electroluminescence quantum efficiency (EQE_{E_{EL}}) of optimal devices measured at different injected currents; (b) J - V plots and (c) EQE curves (solid line) and integrated J_{sc} values (dashed line) of PM6:Y6 and PM6:Y6:BTP-C9-ICT-based optimal devices; (d) V_{oc} - P_{light} and (e) J_{sc} - P_{light} plots for binary and ternary devices.

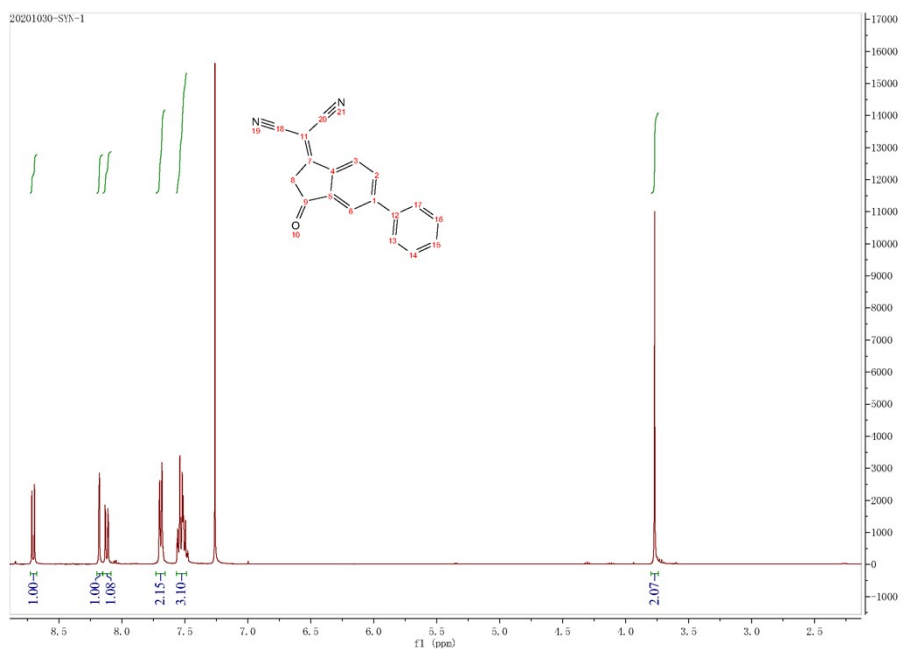
Fig. S9 ^1H NMR.



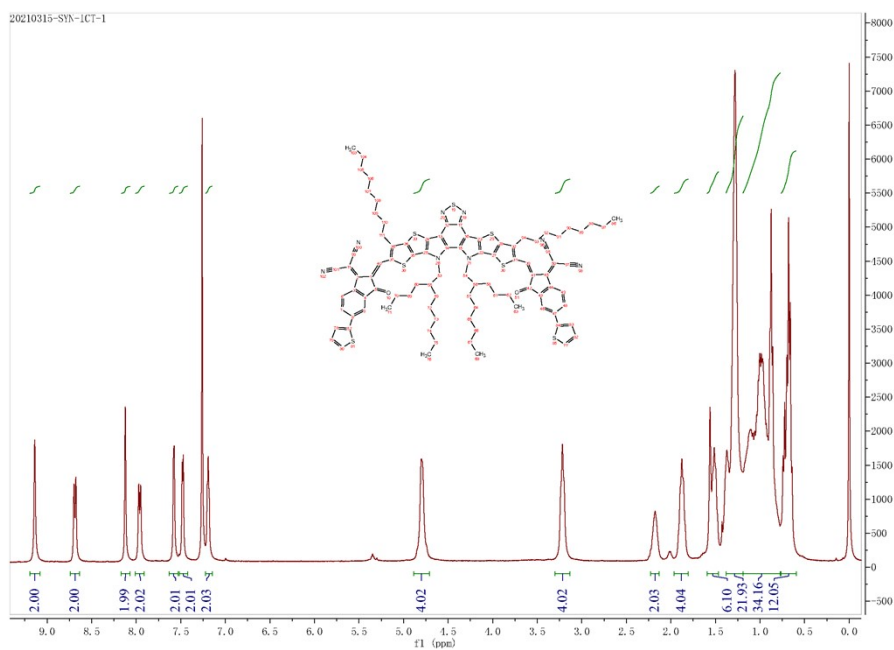
a) ^1H NMR spectrum of compound 3-1.



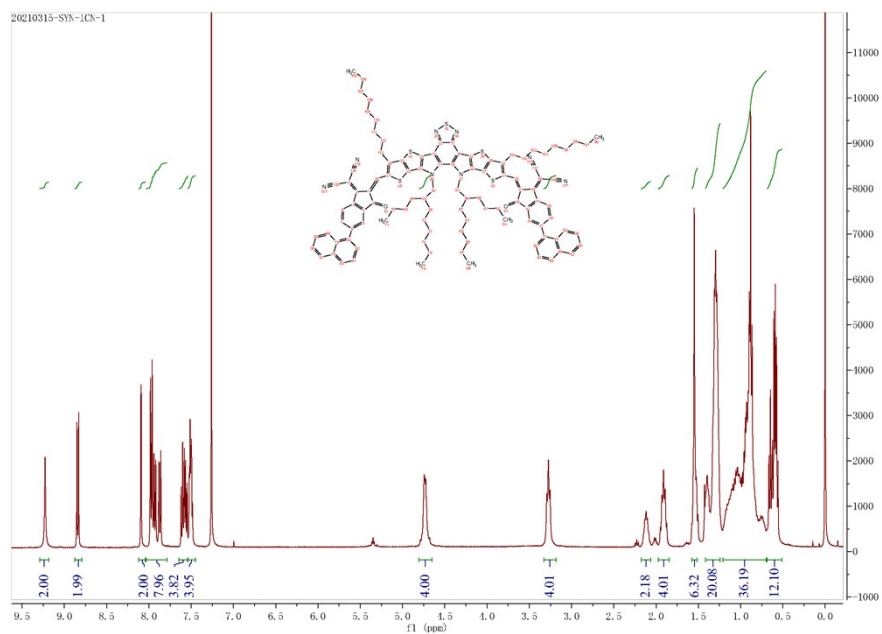
b) ^1H NMR spectrum of compound 3-2.



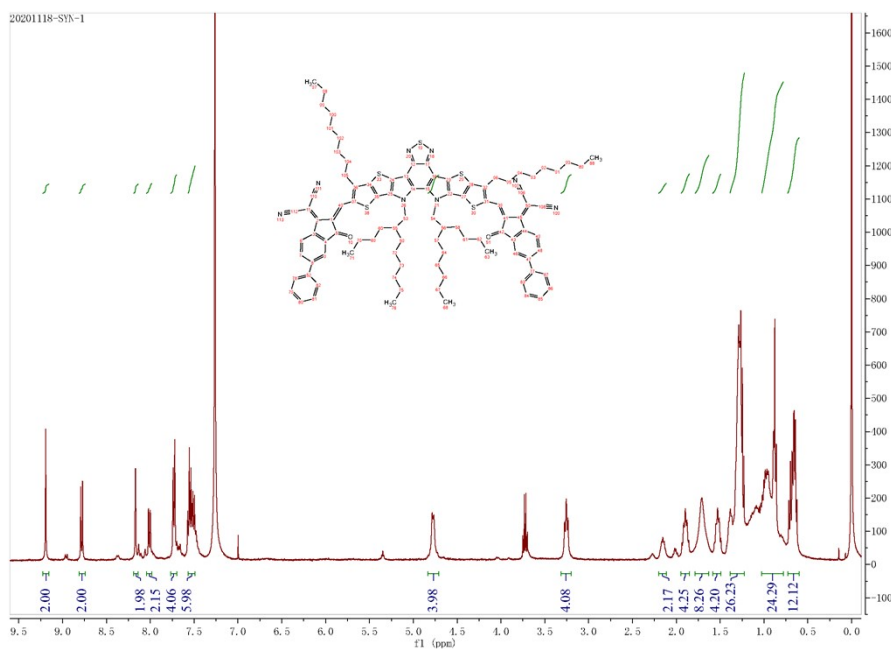
c) ^1H NMR spectrum of compound 3-3.



d) ^1H NMR spectrum of BTP-C9-ICT.



e) ^1H NMR spectrum of BTP-C9-ICN.



f) ^1H NMR spectrum of BTP-C9-ICB.

Table S1 Optical and Electrochemical Properties of Y5 and BTP-C9-ICX.

| Materials | $\lambda_{\text{abs, max}}^{\text{sol}}$ [nm] | $\lambda_{\text{abs, max}}^{\text{film}}$ [nm] | $\lambda_{\text{em, max}}^{\text{film}}$ [nm] | $\Delta\lambda$ [nm] ^{a)} | $\lambda_{\text{abs, edge}}^{\text{film}}$ [nm] | $E_{\text{g}}^{\text{opt}}$ [eV] ^{b)} | $E_{\text{HOMO}}/E_{\text{LUMO}}$ [eV] ^{c)} |
|------------|--|---|--|------------------------------------|--|---|---|
| Y5 | 718 | 782 | 949 | 167 | 900 | 1.38 | -5.58/-3.96 |
| BTP-C9-ICB | 726 | 798 | 907 | 109 | 891 | 1.39 | -5.55/-3.91 |
| BTP-C9-ICN | 726 | 786 | 888 | 102 | 906 | 1.37 | -5.47/-3.87 |
| BTP-C9-ICT | 731 | 790 | 861 | 71 | 880 | 1.41 | -5.50/-3.89 |

a) Stokes-shift values, defined as $\lambda_{\text{em, max}}^{\text{film}} - \lambda_{\text{abs, max}}^{\text{film}}$; b) calculated from $E_{\text{g}}^{\text{opt}} = 1240/\lambda_{\text{abs, edge}}$; c) calculated through CV measurements

Table S2 Detailed photovoltaic performance for PM6-C9-ICT-based OSCs with different total concentration of blend solution, D/A ratio, and thermal annealing temperature.

| Active layer | Concentration | D/A | TA (°C) | V_{oc} (V) | J_{sc} (mA cm ⁻²) | FF (%) | PCE (%) |
|--------------------|---------------|-------|---------|---------------------|---|--------|---------|
| PM6:BTP-C9- ICT | 13 mg/mL | | | 0.991 | 18.24 | 53.44 | 9.66 |
| | 14 mg/mL | 1:1.2 | 110 | 0.993 | 17.43 | 59.60 | 10.32 |
| | 15 mg/mL | | | 0.983 | 17.42 | 55.92 | 9.58 |
| | 14mg/mL | 1:1 | | 0.989 | 18.71 | 54.67 | 10.12 |
| | | 1:1.4 | 110 | 0.990 | 18.99 | 54.00 | 10.15 |
| | 14mg/mL | 1:1.2 | 100 | 0.995 | 15.96 | 58.23 | 9.25 |
| | | | 120 | 0.983 | 16.71 | 58.50 | 9.61 |

Table S3 The electron (μ_e) and hole mobilities (μ_h) for devices.

| Active layers | μ_e (cm ² V ⁻¹ s ⁻¹) | μ_h (cm ² V ⁻¹ s ⁻¹) | μ_h/μ_e |
|----------------|--|--|---------------|
| PM6:BTP-C9-ICB | 6.27×10^{-4} | 1.34×10^{-3} | 2.14 |
| PM6:BTP-C9-ICN | 4.61×10^{-4} | 9.76×10^{-4} | 2.12 |
| PM6:BTP-C9-ICT | 8.08×10^{-4} | 1.57×10^{-3} | 1.94 |

Note: The space charge limited current (SCLC) method was used to measure the (μ_e) and hole mobilities (μ_h) of the blend films. PM6:BTP-C9-ICT blend film exhibited higher charge carrier mobilities and balanced charge transport, which were favourable to efficient carrier collection, leading to the enhancement in FF.

Table S4 The *d*-spacing and the crystalline coherence length (CCL) of the pure and blend films.

| Films | | q (Å ⁻¹) | <i>d</i> -spacing (Å) | FWHM (Å ⁻¹) | CCL (Å) ^{a)} |
|----------------|-------|------------------------|-----------------------|-------------------------|-----------------------|
| Y5 | | 1.715 | 3.66 | 0.205 | 27.58 |
| BTP-C9-ICB | OOP | 1.669 | 3.76 | 0.270 | 20.94 |
| BTP-C9-ICN | (010) | 1.661 | 3.78 | 0.597 | 9.47 |
| BTP-C9-ICT | | 1.710 | 3.67 | 0.155 | 36.48 |
| PM6:Y5 | | 1.708 | 3.68 | 0.186 | 30.40 |
| PM6:BTP-C9-ICB | OOP | 1.672 | 3.76 | 0.216 | 26.18 |
| PM6:BTP-C9-ICN | (010) | 1.668 | 3.77 | 0.223 | 25.36 |
| PM6:BTP-C9-ICT | | 1.708 | 3.68 | 0.200 | 28.17 |

^{a)} The CCLs were calculated according to Scherrer equation: $CCL = 2\pi K / q$, where Δq is the full width at half maximum (FWHM) of the peak and *K* is a shape factor (*K* = 0.9 was used here).

Table S5 The surface energy and Flory–Huggins interaction parameter (χ) of the donor and acceptor materials.

| Donor | Surface energy, γ (mJ m ⁻²) | Acceptors | Surface energy, γ (mJ m ⁻²) | $\chi_{\text{donor-acceptor}}$ |
|-------|---|------------|---|--------------------------------|
| PM6 | 34.47 | BTP-C9-ICB | 44.97 | 0.70K |
| | | BTP-C9-ICN | 44.32 | 0.62K |
| | | BTP-C9-ICT | 43.90 | 0.57K |

Note: Contact angle measurements were employed to evaluate the miscibility between the polymer donor PM6 and these three acceptors. The PM6:BTP-C9-ICT blend film had the lowest Flory–Huggins interaction parameter (χ) of 0.57 K, indicating that the thienyl substituted acceptor BTP-C9-ICT is more miscible with donor PM6, leading to favorable phase separation observed in the microscopic morphology analysis.

Table S6. Total and detailed energy loss (E_{loss}) of optimized devices.

| Devices | E_g^{PV} [eV] ^{a)} | qV_{oc} [eV] | $qV_{\text{oc}}^{\text{SQ}}$ [eV] | $qV_{\text{oc}}^{\text{rad}}$ [eV] | E_{loss} [eV] | ΔE_1 [eV] | ΔE_2 [eV] | ΔE_3 [eV] ^{b)} | EQE _{EL} | cal. ΔE_3 [eV] ^{c)} |
|----------------|---|--------------------------|--------------------------------------|---------------------------------------|---------------------------|-------------------|----------------------|------------------------------------|-----------------------|---|
| PM6:Y5 | 1.47 | 0.95 | 1.20 | 1.13 | 0.52 | 0.27 | 0.07 | 0.18 | 8.60×10 ⁻⁴ | 0.179 |
| PM6:BTP-C9-ICB | 1.48 | 0.98 | 1.21 | 1.13 | 0.50 | 0.27 | 0.08 | 0.15 | 3.42×10 ⁻³ | 0.145 |
| PM6:BTP-C9-ICN | 1.52 | 1.00 | 1.25 | 1.15 | 0.52 | 0.27 | 0.10 | 0.15 | 2.53×10 ⁻³ | 0.153 |
| PM6:BTP-C9-ICT | 1.48 | 0.99 | 1.21 | 1.14 | 0.49 | 0.27 | 0.07 | 0.15 | 2.90×10 ⁻³ | 0.149 |

a) Extracted from the derivative of the EQE spectrum; b) determined by the equation:

$$\Delta E_3 = qV_{\text{oc}}^{\text{rad}} - qV_{\text{oc}}; \text{ c) calculated from EQE}_{\text{EL}} \text{ measurements: } \Delta E_3 = -kT \ln(\text{EQE}_{\text{EL}}).$$

Table S7 The PLQY values for pure and blend films of BTP-C9-ICX.

| Pure/Blend films | PLQY (%) ^{a)} |
|---------------------------|------------------------|
| Y5/PM6:Y5 | 3.76/1.93 |
| BTP-C9-ICB/PM6:BTP-C9-ICB | 7.44/2.69 |
| BTP-C9-ICN/PM6:BTP-C9-ICN | 5.46/2.54 |
| BTP-C9-ICT/PM6:BTP-C9-ICT | 6.93/2.62 |

^{a)} Measured from the integrating sphere method.

Table S8 Photovoltaic parameters for OSCs with low ΔV_{nr} (≤ 0.16 V).

| Active layers | V_{oc} (V) | J_{sc} (mA cm ⁻²) | FF (%) | PCE (%) | ΔV_{nr} (V) | Ref. |
|-----------------|--------------|------------------------------------|--------|---------|---------------------|---------------|
| PBT1-C-2Cl:BTA3 | 1.30 | 6.42 | 46.5 | 3.9 | 0.16 | ⁹ |
| PTB7-Th:SPA1 | 1.15 | 8.87 | 43.6 | 4.46 | 0.16 | ¹⁰ |
| 10k_PM6:Y16F | 0.922 | 14.50 | 38.8 | 5.2 | 0.155 | ¹¹ |
| PBDB-T:SM16-R | 0.977 | 19.00 | 60.02 | 11.14 | 0.145 | ¹² |
| PM6:SN | 0.82 | 25.14 | 68.9 | 14.3 | 0.15 | ¹³ |
| PM6:BTP-C9-ICB | 0.98 | 12.25 | 57.34 | 6.88 | 0.145 | this work |
| PM6:BTP-C9-ICN | 1.00 | 13.62 | 56.98 | 7.76 | 0.153 | this work |
| PM6:BTP-C9-ICT | 0.99 | 17.49 | 65.95 | 11.42 | 0.149 | this work |

Table S9 Photovoltaic parameters of the ternary OSCs based on PM6:Y6:BTP-C9-ICT blends with different weight percentage of BTP-C9-ICT.

| Active Layers | V_{oc} (V) | J_{sc} (mA cm ⁻²) | FF (%) | PCE (%) ^{a)} |
|--------------------------|--------------|---------------------------------|--------|-----------------------|
| PM6:Y6 | 0.842 | 24.74 | 75.87 | 15.80 (15.66) |
| PM6:Y6:BTP-C9-ICT(10wt%) | 0.855 | 25.72 | 75.43 | 16.59 (16.37) |
| PM6:Y6:BTP-C9-ICT(20wt%) | 0.868 | 24.58 | 70.80 | 15.12 (14.95) |
| PM6:Y6:BTP-C9-ICT(30wt%) | 0.880 | 22.14 | 71.33 | 13.90 (13.76) |
| PM6:Y6:BTP-C9-ICT(50wt%) | 0.912 | 23.08 | 69.68 | 14.65 (14.38) |
| PM6:Y6:BTP-C9-ICT(70wt%) | 0.937 | 21.6 | 64.02 | 12.96 (12.64) |
| PM6:Y6:BTP-C9-ICT(90wt%) | 0.957 | 20.18 | 60.37 | 11.66 (11.38) |

^{a)} The average values in the parentheses were obtained from 10 devices.

Note: After the incorporation of 10wt% BTP-C9-ICT, the ternary device yielded an improved PCE (16.59% vs 15.80%), which was ascribed to the simultaneously increased V_{oc} (0.855 vs 0.842 V) and J_{sc} (25.72 vs 24.74 mA cm⁻²) and the maintained FF (75.43% vs 75.87%). Moreover, the ternary device possessed weaker trap-assisted and bimolecular recombination for charge carriers than binary one (Fig. S8d, e). These results indicated that NFAs with low energy loss is the potential third component to fine-tune the energy level alignment and enhance the photovoltaic performance of OSCs.

References

- 1 D. K. Owens and R. C. WENDT, *J. Appl. Polym. Sci.*, 1969, **13**, 1741-1747.
- 2 S. Nilsson, A. Bernasik, A. Budkowski and E. Moons, *Macromolecules*, 2007, **40**, 8291-8301.
- 3 J. Yao, T. Kirchartz, M. S. Vezie, M. A. Faist, W. Gong, Z. He, H. Wu, J. Troughton, T. Watson, D. Bryant and J. Nelson, *Phys. Rev. Appl.*, 2015, **4**, 014020.
- 4 Y. Wang, D. Qian, Y. Cui, H. Zhang, J. Hou, K. Vandewal, T. Kirchartz and F. Gao, *Adv. Energy Mater.*, 2018, **8**, 1801352.
- 5 J. Liu, S. Chen, D. Qian, B. Gautam, G. Yang, J. Zhao, J. Bergqvist, F. Zhang, W. Ma, H. Ade, O. Inganäs, K. Gundogdu, F. Gao and H. Yan, *Nat. Energy*, 2016, **1**, 16089.
- 6 S. Liu, J. Yuan, W. Deng, M. Luo, Y. Xie, Q. Liang, Y. Zou, Z. He, H. Wu and Y. Cao, *Nat. Photonics*, 2020, **14**, 300-305.

- 7 U. Rau, *Phys. Rev. B*, 2007, **76**, 085303.
- 8 S. D. Stranks, R. L. Z. Hoye, D. Di, R. H. Friend and F. Deschler, *Adv. Mater.*, 2018, **31**, 1803336.
- 9 N. An, Y. Cai, H. Wu, A. Tang, K. Zhang, X. Hao, Z. Ma, Q. Guo, H. S. Ryu, H. Y. Woo, Y. Sun and E. Zhou, *Adv. Mater.*, 2020, **32**, 2002122.
- 10 H. Sun, B. Liu, J. Yu, X. Zou, G. Zhang, Y. Zhang, W. Zhang, M. Su, Q. Fan, K. Yang, J. Chen, H. Yan, F. Gao and X. Guo, *Sci. China Chem.*, 2020, **63**, 1785-1792.
- 11 Q. Liu, S. Smeets, S. Mertens, Y. Xia, A. Valencia, J. D'Haen, W. Maes and K. Vandewal, *Joule*, 2021, **5**, 2365-2379.
- 12 H. Lu, W. Liu, H. Jin, H. Huang, Z. Tang and Z. Bo, *Adv. Funct. Mater.*, 2021, DOI: 10.1002/adfm.202107756, 2107756.
- 13 W. Liu, S. Sun, L. Zhou, Y. Cui, W. Zhang, J. Hou, F. Liu, S. Xu and X. Zhu, *Angew. Chem. Int. Ed.*, 2021, DOI: 10.1002/anie.202116111.